



Macroscopic simulations of the SiC thermal oxidation process based on the Si and C emission model

Yasuto Hijikata

Graduate School of Science and Engineering, Saitama University, Saitama 338-8570, Japan

ARTICLE INFO

Keywords:

4H-SiC
Oxidation
MOS interfaces
Interface state density
Si and C emission
Active/passive oxidation

ABSTRACT

The interface defects formed at the oxide–SiC interface impact not only on channel mobility of MOSFET but also on many scenes such as generation or extinction of Si/C atom vacancies and formation of single-photon sources. Therefore, it is very important to know the oxidation mechanism of SiC more in detail. We have previously proposed a unified SiC oxidation model based on the Si and C emission phenomenon. In addition, it has been revealed that this model accurately reproduces the oxide growth rate in the entire oxide thickness range for various oxidation conditions and substrate surface orientations. In this report, based on the experimental verifications for the four oxidation stages deduced from this unified oxidation model, the validity of this model was reviewed. Furthermore, the interface-emitted Si and C concentrations were simulated for various oxidation temperatures and substrate surface orientations. Based on the simulation results together with experimental results of interface state density, the optimum oxide growth condition has been discussed.

1. Introduction

To deeply understand the thermal oxidation mechanism of silicon carbide (SiC) is very important not only for the improvement in low-power-loss performance and high-reliability of metal-oxide-semiconductor field-effect-transistors (MOSFETs) but for the performance of bipolar devices. The reason for former is closely relevant to reducing interface state density of the oxide–SiC interface [1] and the later one is because the carrier lifetime is improved [2] by elucidating the SiC oxidation mechanism. Also in the recent study, it has been reported that stacking faults, which degrade the forward electrical current [3], are formed at the epilayer/bulk interface [4] after a relatively long-term oxidation [5]. Furthermore, it has been reported that oxidation of SiC substrate brings about the formation of single-photon sources near the oxide–SiC interface [6–8]. We have attempted to acquire some information about the SiC thermal oxidation mechanism by performing real-time monitoring of the oxide growth on SiC substrates using an in-situ spectroscopic ellipsometer. As a result of real-time growth rate measurements, we found that the growth rate rapidly decreased in the initial stage of oxidation [9–11]. This initial deceleration of growth rate has also been pointed by the others [12,13]. In addition, we proposed a kinetic model, termed “Si and C emission model” [14] (SCEM), that accounts for this initial oxidation deceleration, and succeeded in reproduction of the observed growth rates generally in the whole thickness region. Moreover, oxide growth rates for various crystal

orientations, oxidation temperatures, and oxygen partial pressures were successfully reproduced using the SCEM, evidencing the validity of SCEM [15,16]. The fitting parameters deduced from the calculations revealed that: The activation energy of maximum surface reaction rate corresponds to the number of Si backbonds for each surface orientation; The difference in growth rate is chiefly attributed to the difference in the Si emission ratio. Based on the obtained information on SiC oxidation process, we categorized the SiC oxidation into four stages, as will be described in next section.

In this paper, I review the validity of the four oxidation stages of SCEM in the light of the experimental results recently obtained as well as the reproduction of oxide growth rate.

2. Oxide growth processes

Based on information from the real time observations and the model calculations of the oxide growth on SiC substrates, we inferred that there were four stages in the SiC oxidation process [16]. Fig. 1 exhibits a scheme of the SiC oxidation rate in the whole oxide thickness regime. The details of these four oxidation stages are as follows: i) Oxide growth on the surface (*active oxidation* [17]) is dominant; ii) Interface oxidation reaction rate reducing, iii) Oxidation rate deceleration settled, iv) Transferring to the oxygen in oxide diffusion-limited rate. In stage i), since most of the emitted interstitials (Si and C) are segregated on the oxide surface and are rapidly oxidized, interstitials are hardly

E-mail address: yasuto@opt.ees.saitama-u.ac.jp.

<https://doi.org/10.1016/j.diamond.2019.01.012>

Received 28 September 2018; Received in revised form 11 January 2019; Accepted 17 January 2019

Available online 18 January 2019

0925-9635/ © 2019 Elsevier B.V. All rights reserved.

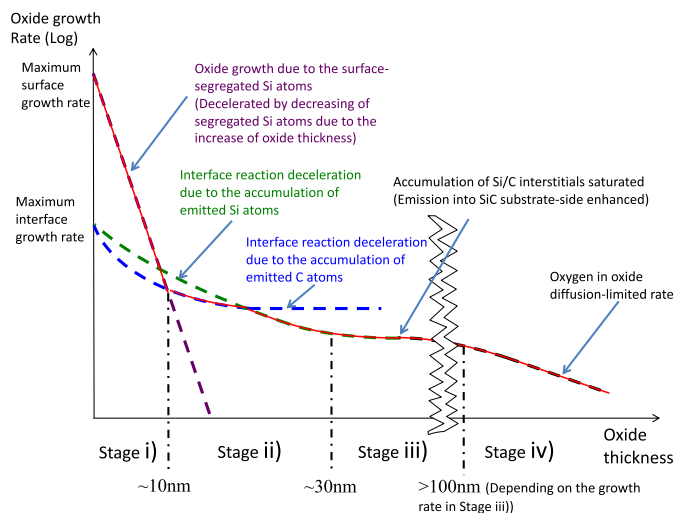


Fig. 1. Schematic illustration of the SiC oxidation rate in the entire thickness region.

accumulated near the oxidation interface. From stage ii), the interface oxidation reaction (*passive oxidation*) is dominant and thereby interface reaction rate is reduced due to the accumulation of interstitial near the oxidation interface. Because the solubility limit of SiO₂ is much higher than that of SiC, the emissions into the oxide are dominant in the beginning of Stage ii). However, when the accumulation of interstitial in SiO₂ is saturated (stage iii)), the emission into SiC begins to increase. Still, the accumulation of C interstitial hardly occurs because of its high diffusivity. On the other hand, the accumulation of Si interstitial just inside SiC layer begins from stage iii), which has been confirmed by the oxidation process simulations (Section 4). In stage iv), since the oxide growth rate is reduced due to the oxygen diffusion-limited rate, also the emission rates of interstitials are reduced.

3. Evidences for the oxidation stages

In this section, each stage i)–iv) mentioned in Section 2 will be evidenced based on the experimental data.

3.1. Oxide surface growth: stage i)

It has been found that the growth rates at the very early stage are remarkably high [18,19]. Especially in the case of low-pressure oxidation, the growth rates cannot be explained by the Si emission model for Si oxidation [20,21], as well as by the SCEM for SiC oxidation [15,16]. Accordingly, we performed the measurements of oxide growth rate on 4H-SiC substrates at various oxygen-partial pressures using an in-situ spectroscopic ellipsometer [15]. In general, wide bandgap semiconductors such as a 4H-SiC are transparent at a wide range of the visible wavelength region. In this case, the angle of incidence should be set to the Brewster angle to improve the accuracy of oxide thickness. In the case of 4H-SiC, the Brewster angle is about 70°. However, once oxide growth starts, the Brewster angle increases with increasing oxide thickness. Accordingly, we selected an angle of incidence of 75°, which was optimized for monitoring the oxide growth on 4H-SiC. Fig. 2 shows the oxide growth rates at various oxygen-partial pressures [16]. As can be seen from the figure, the growth rates are much higher than the growth rate curves calculated by the Si and C emission model (broken lines.) We considered that this discrepancy was due to the oxidation rates insufficiently introduced with the surface oxidation. Accordingly, by introducing an additional surface oxidation term to the growth rate equation, we attempted to reproduce the growth rates at the very early stage correctly [16]. As revealed by the solid lines in Fig. 2, the observed growth rates were successfully reproduced by this modification,

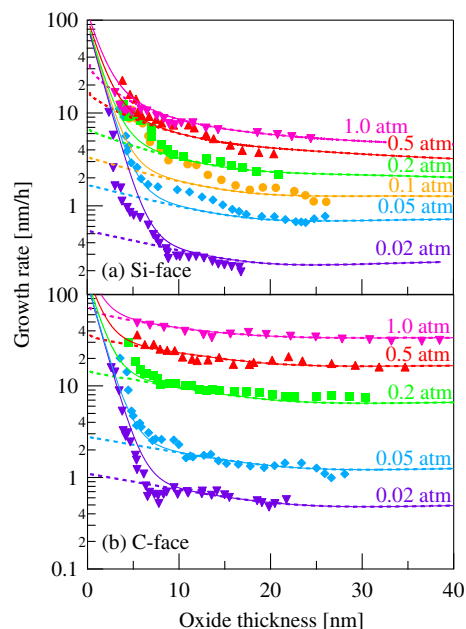


Fig. 2. Dependence of the oxide thickness on the growth rates for the (a) Si-face and (b) C-face at various oxygen-partial pressures and 1100 °C. The solid and dashed curves represent growth rates calculated using the Si and C emission model with and without modified surface oxide growth rate, respectively. Source: Reproduced from [16]. CC BY 3.0.

evidencing the presence of the enhanced surface oxide growth.

Furthermore, the Si and C emission into the oxide layer during the oxidation and the SiO₂ growth on the oxide surface were confirmed from the depth profiles of oxidized HfO₂/SiC structures. A HfO₂ layer of 5.6 nm thickness was deposited on a SiC Si-face epi-substrate. The samples were oxidized in ¹⁸O ambient of 10 Pa pressure at the temperature of 1000 °C. Fig. 3 shows depth profiles of ¹⁸O, SiC, ¹⁸⁰Hf¹⁶O₂, C, Si₂¹⁸O₅ (equivalent to Si¹⁸O₂), Si₂¹⁸O (equivalent to a sub-oxide), and HfO₂ for 1 min of oxidation (a) and 10 min of oxidation (b) obtained by time-of-flight secondary ion mass spectroscopy (TOF-SIMS) [22]. The results surely confirm the Si emission and the SiO₂ growth on the oxide surface. However, the presence of C emission was identified as a small amount of HfC₂ in the sample surface and not a few amounts of HfC₂ around the Si₃O–SiC interface which is due to the reaction of C and Hf. A very recent report identified the C emission into the oxide layer after post-oxidation Ar annealing [23]. It is likely that the C emission occurs during oxidation as well as during post-oxidation annealing because the C (or CO) interstitial diffusion becomes faster when the interstitials encounter coming oxygen and thereby they rapidly escape from the oxide.

We also performed angle-resolved X-ray photoemission spectroscopy (AR-XPS) for the oxide films grown by 1, 10, 60, or 180 min of oxidation. Fig. 4 shows the schematic illustrations of the HfO₂/SiC structure during initial oxidation and the multi-oxide-layer structures after the oxidation deduced from the TOF-SIMS analyses. A HfO₂ film of 2.8 nm thickness was deposited on a SiC Si-face epi-substrate. The oxidations were carried out at the temperature of 1100 °C and atmospheric pressure. Here, the multi-layer structure at right end was assumed for the AR-XPS analyses. Photoemission spectra in the O1s region were used to derive the thicknesses of the multi-layer structure. The details on the analysis were presented elsewhere [22].

Fig. 5 shows the thicknesses of the multi-layer structure as a function of oxidation time obtained from the AR-XPS analyses. The thicknesses d_1 and d_2 are surface oxide thickness and interface oxide thickness, respectively, shown by Fig. 4. The results indicated that the oxidation process actually followed the process illustrated in Fig. 4. Namely, only the surface growth is dominant at the very early stage and

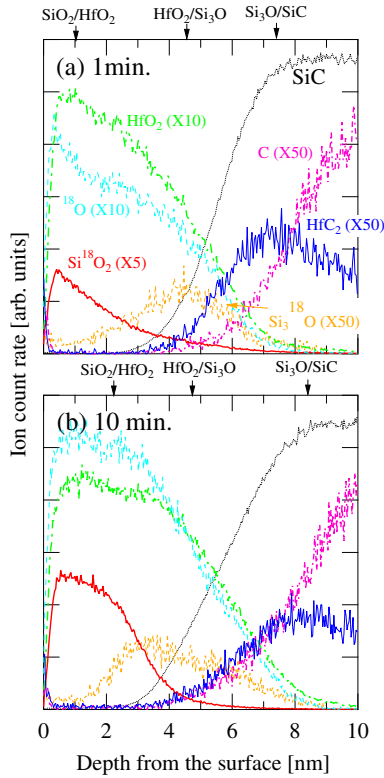


Fig. 3. Depth profiles of ^{18}O , SiC, $^{180}\text{Hf}^{16}\text{O}_2$, C, $\text{Si}_2^{18}\text{O}_5$, Si_2^{18}O , and HfC_2 for 1 min oxidation (a) and 10 min oxidation (b).

then, the surface growth is calmed down and the interface oxide growth predominantly progresses.

The above-mentioned three experimental results indicated that the Si and C interstitials emit into the oxide layer during oxidation and the surface oxide growth prominently occurs at the very early stage.

3.2. Interfacial reaction rate deceleration: stage ii)

According to the Si emission model [24] and the Si and C emission model [14], the initial growth rate deceleration of Si/SiC oxidation is due to the deceleration of interface reaction rate, which is induced by the accumulation of Si (and C) interstitials emitted during oxidation. To describe the deceleration of the interface reaction rate, these decreasing functions, k , were given for the Si and SiC oxidation [14,24]:

$$k = k_0 \left(1 - \frac{C_{\text{Si}}^i}{C_{\text{Si}}^0} \right) \quad (\text{for Si}),$$

$$k = k_0 \left(1 - \frac{C_{\text{Si}}^i}{C_{\text{Si}}^0} \right) \left(1 - \frac{C_{\text{C}}^i}{C_{\text{C}}^0} \right) \quad (\text{for SiC}),$$

(1)

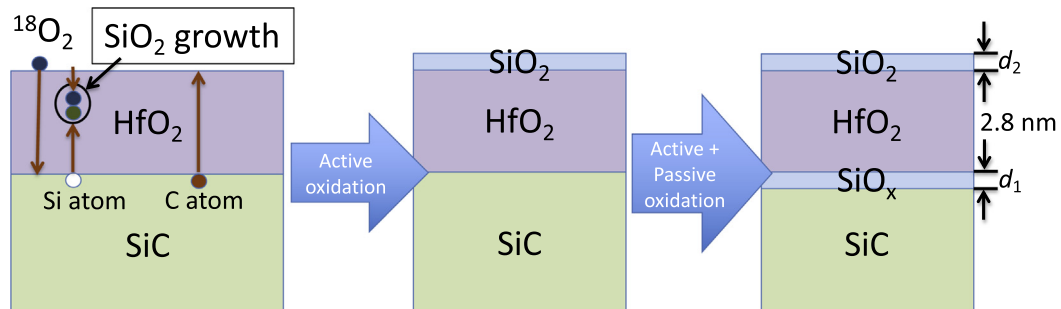


Fig. 4. Schematic illustrations of the HfO_2/SiC structure and the multi-oxide-layer structures after oxidation. The structure at right end was assumed for the AR-XPS analyses.

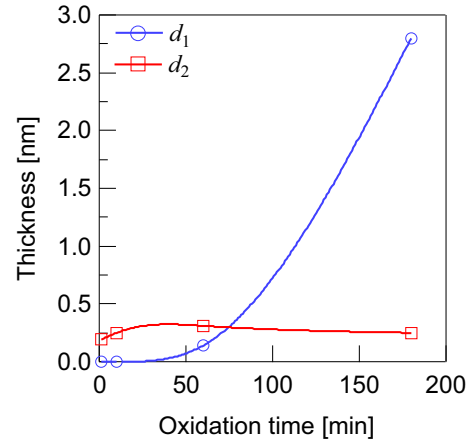


Fig. 5. Thickness of the multi-layer structure as a function of the oxidation time. d_n is the thickness shown in Fig. 4. The solid lines are spline curves for the observed data.

where k_0 , C^i , and C^0 are the initial interfacial reaction rate, the concentrations at the SiC– SiO_2 interface, the solubility limits in SiO_2 , respectively, and the subscript means the value for the corresponding atom. That is, it is assumed that the solubility limit is the maximum concentration of interstitial and the k is negatively proportional to the concentration of interstitial. Here, in the case of SiC oxidation, decreasing terms for Si and C interstitials were given because the SiC oxidation involves the emissions of Si and C interstitials as revealed in the previous section.

To prove the interfacial reaction rate deceleration and the validity of Eq. (1), we carried out two kinds of test experiments: Real-time measurements of the re-oxidation rate after Ar annealing and two-temperature (two-step) oxidation [22].

A scheme of the growth rate curves with and without Ar annealing is shown at the left-side in Fig. 6, where d_a and Δv are the annealed oxide thickness and the recovery rate, respectively. Since such a thermal treatment without oxidation reaction (i.e. Ar annealing) enhances diffusion of interstitials, the value of C^i should be reduced, leading to the increase in interfacial reaction rate k . Here, we assume that Δv increases exponentially to the maximum recovery rate (Δv_{max}) with a recovery time constant τ , i.e.,

$$\Delta v = \Delta v_{\text{max}} (1 - \exp(-t/\tau))$$

(2)

Fig. 6 shows the parameters for Eq. (2) as a function of the annealed thickness obtained from curve fitting. SiC Si-face epi-layers were used in this experiment. The Ar annealing temperature was 1050 or 1150 °C. We see from the figure that the maximum recovery rate is almost proportional to the annealed thickness but scarcely depends on oxidation temperature. Conversely, the recovery time constant depends not on d_a but on oxidation temperature. Therefore, it is reasonable to

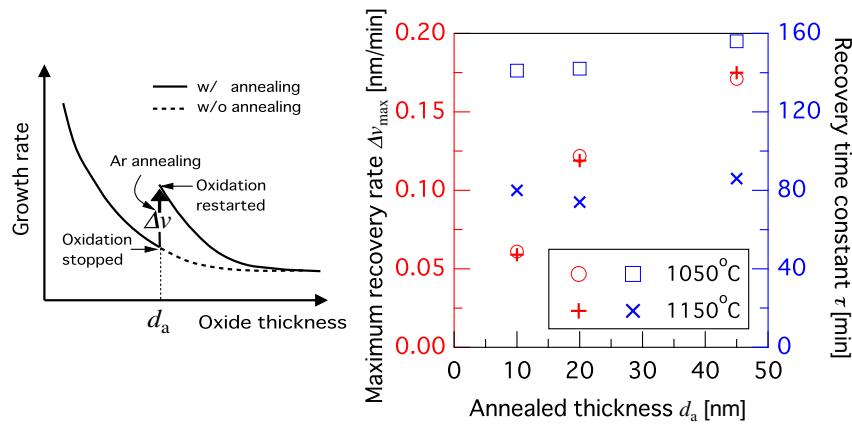


Fig. 6. A scheme of the growth rate curves with and without Ar annealing (left side) and parameters for Eq. (2) as a function of the annealed thickness obtained from curve fitting (right side).

consider that the interface-accumulated Si and/or C interstitials were diffused by the thermal treatment.

Next, consider the results from two-temperature measurements. Obviously, the lower oxidation temperature, the lower C^I . Hence, we expect the results of the two-temperature measurements as follows (here, the initial temperatures are various ones and the second temperature is common): the growth rate of the sample that underwent lowest initial oxidation temperature is the highest when switching to second oxidation temperature. Fig. 7 exhibits the oxide growth rates as a function of oxide thickness at various initial oxidation temperatures. SiC Si-face epi-layers were used in this experiment. It can be seen from the figure that just in the beginning of oxidation, oxide growth rate is extremely high and then rapidly decreases. Because the bare SiC substrate actively incorporates oxygen, once the surface is covered with reacted oxygen, the oxidized layer itself prevents the oxide growth. As expected, the lower oxidation temperature at the initial oxidation, the higher growth rate at the second oxidation. The result also confirms that the growth rates converge to a common rate after the accumulation of interstitials are saturated, i.e. at stage iii).

These experimental results are strong indication that evidences the validities of the interfacial reaction rate deceleration and Eq. (1). Also, it is suggested that the concentrations of Si and/or C interstitial at the oxidation interface are eliminated by a smaller oxide thickness or a lower oxidation temperature. The simulations for densities of Si and C interstitials at the interface will be presented in Section 4.

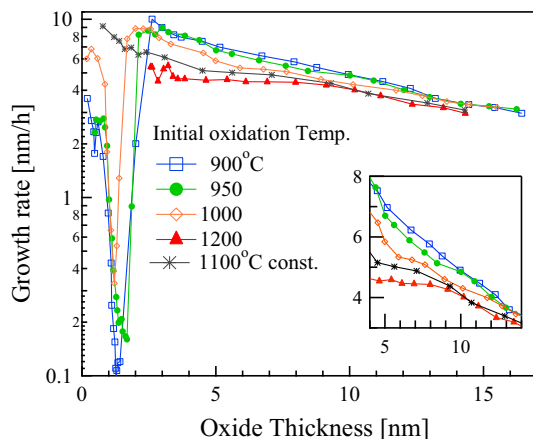


Fig. 7. Oxide growth rates as a function of oxide thickness at various initial oxidation temperatures. The second step oxidation temperature was 1100 °C for all samples. The inset denotes growth rate data restricted to the second oxidation.

Source: Reproduced from [22]. CC BY 3.0.

3.3. Linear and parabolic oxide growth: stage iii) & iv)

It is well-known that a linear-parabolic oxide growth equation, so-called Deal-Grove model [25], well reproduce the oxide growth rate of Si at the thicknesses more than a few 10 nm. Several studies pointed out that this model is also applicable to the SiC oxidation in this thickness range [13,26–28]. Since the Deal-Grove model assumes a series oxidation reaction in which the constant interface reaction is dominant in the thin oxide regime followed by the oxygen diffusion rate-limiting in the thick oxide regime, it is clear that this model is identical to the above-mentioned stage iii) and iv). Therefore, the validity of Stage iii) and iv) was evidenced.

4. Macroscopic simulations

So far the validity of the Si and C emission model has been verified. Consequently, its validity was revealed in all the oxide thickness region and oxidation conditions (i.e. oxidation temperature, oxygen-partial-pressure, substrate surface orientation, ...). On the other hand, it is obvious that the concentrations of Si and C interstitials are closely related to the density of interface traps. Accordingly, we carried out the simulations of concentrations of Si and C interstitials for various oxidation conditions so as to establish a structure-optimized guideline of MOS interface on a calculator using this model. Although I have described only the concentrations of Si and C interstitials at oxide-side (C_{Si}^I and C_C^I in Eq. (1)), the concentrations at the SiC-side are also important because the carriers actually run in the SiC-side. Accordingly, we also obtained the concentrations of Si and C interstitials at the SiC-side by performing simulations using diffusion theory. The calculation method in detail is found elsewhere [16].

Fig. 8 shows dependence of the oxide thickness on the Si and C interstitial concentrations at the interface with the Si-face, a-face and C-face at various oxidation temperatures and 1.0 atm, where C^{Ib} denotes the concentrations at the SiC-side. It is noticed that, in the case of Si interstitial, the higher temperature gives rise to the lower concentration at the initial stage of oxide-side and at the entire stage of SiC-side. According to the report from Hosoi et al [29], the oxidation temperature dependence of interface state density exhibits that the higher temperature corresponds to the lower interface state density. In comparison between 1150 °C and 1200 °C, the interface state density is reduced by a factor of several 10%, which is coincidence with the concentration of Si interstitial at the SiC-side. In addition, only in the case of Si-face, decreasing of concentration at the oxide-side corresponding to the diffusion rate-limiting step was not clearly seen. Therefore, the higher temperature and thinner oxide are superior to reduce Si-related defect such as NIT [30].

For C interstitial, the results for oxide-side clearly exhibited a

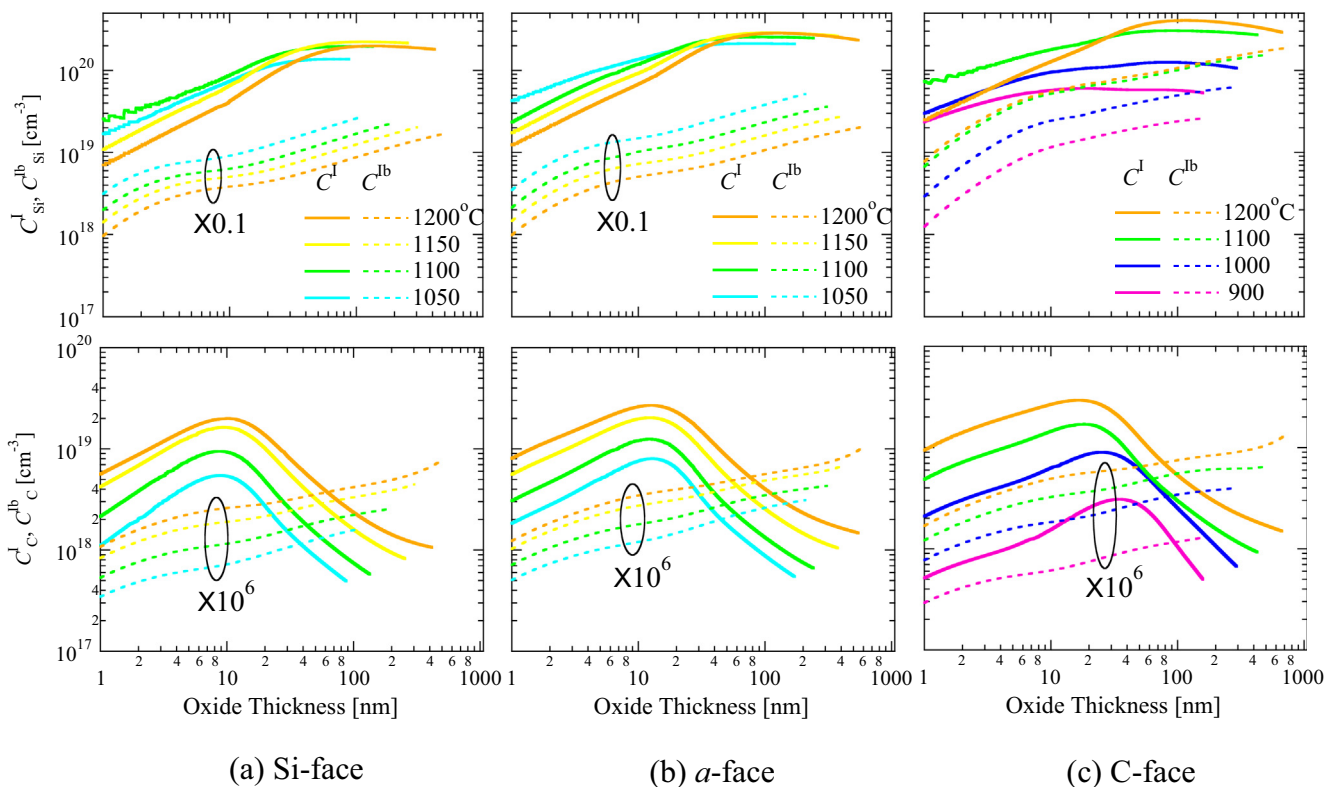


Fig. 8. Dependence of the oxide thickness on the Si and C interstitial concentrations at the interface with the (a) Si-face, (b) a-face and (c) C-face at various oxidation temperatures and 1.0 atm. The solid and dashed curves represent the concentrations on the oxide side (C^I) and substrate side (C^{Ib}), respectively. Source: Reproduced from [16]. CC BY 3.0.

maximum around a few 10 nm. While in the SiC-side, the concentrations showed a monochromatic increase with increasing oxide thickness and an increase in whole of thickness region with elevating temperature. Although the concentrations at SiC-side were several orders lower than those at oxide-side, it is possible that the C interstitials at SiC-side react to each other to be immobile defects and these defects accumulate at the interface, as proposed by Shen and Pantelides [31]. Anyway, it is predicted that a thinner oxide grown at lower temperature is appropriate to the reduction of C-related defect (e.g. C cluster [30].)

5. Conclusion

The four oxidation stages included in the SiC thermal oxidation model which we previously proposed were experimentally verified. As a result, these four oxidation stages were completely evidenced. The simulations of Si and C interstitial concentrations at the oxidation interface as a function of oxide thickness on various oxidation temperatures and substrate surface orientation were performed using the SiC oxidation model. Based on the simulation results, a guideline that establishes the oxide formation recipe for reducing the SiC MOS interface defect could be obtained.

Acknowledgement

This work was supported in part by Grants-in-Aid for Scientific Research (15H03967, 17H01056, 18H03770) from the Japan Society for the Promotion of Science.

References

- [1] T. Kimoto, Material science and device physics in SiC technology for high-voltage power devices, *Jpn. J. Appl. Phys.* 54 (2015) 040103.
- [2] T. Hiyoshi, T. Kimoto, Elimination of the major deep levels in n- and p-type 4H-SiC by two-step thermal treatment, *Appl. Phys. Express* 2 (2009) 091101.
- [3] H. Lendenmann, F. Dahlquist, N. Johansson, R. Soderholm, P.A. Nilsson, J.P. Bergman, P. Skytt, Long term operation of 4.5 kV PIN and 2.5 kV JBS diodes, *Mater. Sci. Forum* 727 (2001) 353–356.
- [4] R. Asafuji, Y. Hijikata, Generation of stacking faults in 4H-SiC epilayer induced by oxidation, *Mater. Res. Express* 5 (2018) 015903.
- [5] Y. Miyano, R. Asafuji, S. Yagi, Y. Hijikata, H. Yaguchi, Photoluminescence study of oxidation-induced faults in 4H-SiC epilayers, *AIP Adv.* 5 (2015) 127116.
- [6] A. Lohmann, S. Castelletto, J.R. Klein, T. Ohshima, M. Bosi, M. Negri, D.W.M. Lau, B.C. Gibson, S. Praver, J.C. McCallum, B.C. Johnson, Activation and control of visible single defects in 4H-, 6H-, and 3C-SiC by oxidation, *Appl. Phys. Lett.* 108 (2016) 021107.
- [7] S.-i. Sato, T. Honda, T. Makino, Y. Hijikata, S.-Y. Lee, T. Ohshima, Room temperature electrical control of single photon sources at 4H-SiC surface, *ACS Photon.* 5 (2018) 3159.
- [8] Y. Hijikata, T. Horii, Y. Furukawa, Y.-i. Matsushita, T. Ohshima, Oxygen-incorporated single-photon sources observed at the surface of silicon carbide crystals, *J. Phys. Commun.* 2 (2018) 111003.
- [9] T. Yamamoto, Y. Hijikata, H. Yaguchi, S. Yoshida, Growth rate enhancement of (000-1)-face silicon-carbide oxidation in thin oxide regime, *Jpn. J. Appl. Phys.* 46 (2007) L770.
- [10] T. Yamamoto, Y. Hijikata, H. Yaguchi, S. Yoshida, Oxide growth rate enhancement of silicon carbide (0001) Si-faces in thin oxide regime, *Jpn. J. Appl. Phys.* 47 (2008) 7803.
- [11] D. Goto, Y. Hijikata, S. Yagi, H. Yaguchi, Differences in SiC thermal oxidation process between crystalline surface orientations observed by *in-situ* spectroscopic ellipsometry, *J. Appl. Phys.* 117 (2015) 095306.
- [12] V. Šimonka, A. Hössinger, J. Weinbub, S. Selberherr, Growth rates of dry thermal oxidation of 4H-silicon carbide, *J. Appl. Phys.* 120 (2016) 135705.
- [13] E.A. Ray, J. Rozen, S. Dhar, L.C. Feldman, J.R. Williams, Pressure dependence of SiO₂ growth kinetics and electrical properties on SiC, *J. Appl. Phys.* 103 (2008) 023522.
- [14] Y. Hijikata, H. Yaguchi, S. Yoshida, A kinetic model of silicon carbide oxidation based on the interfacial silicon and carbon emission phenomenon, *Appl. Phys. Express* 2 (2009) 021203.
- [15] Y. Hijikata, S. Yagi, H. Yaguchi, S. Yoshida, Model calculations of SiC oxide growth rates at sub-atmospheric pressures using the Si and C emission model, *Mater. Sci. Forum* 740–742 (2013) 833.
- [16] D. Goto, Y. Hijikata, Unified theory of silicon carbide oxidation based on the Si and C emission model, *J. Phys. D. Appl. Phys.* 49 (2016) 225103.
- [17] N.S. Jacobson, D.L. Myers, Active oxidation of SiC, *Oxid. Met.* 75 (2011) 1–25.
- [18] K. Kouda, Y. Hijikata, S. Yagi, H. Yaguchi, Oxygen partial pressure dependence of the SiC oxidation process studied by *in-situ* spectroscopic ellipsometry, *J. Appl. Phys.*

- Phys. 112 (2012) 024502.
- [19] G.H.S. Dartora, E. Pitthan, F.C. Stedile, Unraveling the mechanisms responsible for the interfacial region formation in 4H-SiC dry thermal oxidation, *J. Appl. Phys.* 122 (2017) 215301.
- [20] J. Farjas, P. Roura, Oxidation of silicon: further tests for the interfacial silicon emission model, *J. Appl. Phys.* 102 (2007) 054902.
- [21] T. Christen, A. Ioannidis, C. Winkelmann, A model for thermal oxidation of Si and SiC including material expansion, *J. Appl. Phys.* 117 (2015) 084501.
- [22] Y. Hijikata, R. Asafuji, R. Konno, Y. Akasaka, R. Shinoda, Si and C emission into the oxide layer during the oxidation of silicon carbide and its influence on the oxidation rate, *AIP Adv.* 5 (2015) 067128.
- [23] T. Kobayashi, T. Kimoto, Carbon ejection from a SiO₂/SiC(0001) interface by annealing in high-purity Ar, *Appl. Phys. Lett.* 111 (2017) 062101.
- [24] H. Kageshima, K. Shiraishi, M. Uematsu, Universal theory of Si oxidation rate and importance of interfacial Si emission, *Jpn. J. Appl. Phys.* 38 (1999) L971.
- [25] B.E. Deal, A.S. Grove, General relationship for the thermal oxidation of silicon, *J. Appl. Phys.* 36 (1965) 3770.
- [26] Y. Song, S. Dhar, L.C. Feldman, G. Chung, J.R. Williams, Modified Deal Grove model for the thermal oxidation of silicon carbide, *J. Appl. Phys.* 95 (2004) 4953.
- [27] E. Szilágyi, P. Petrik, T. Lohner, A.A. Koós, M. Fried, G. Battistig, Oxidation of SiC investigated by ellipsometry and Rutherford backscattering spectrometry, *J. Appl. Phys.* 104 (2008) 014903.
- [28] R.H. Kikuchi, K. Kita, Interface-reaction-limited growth of thermal oxides on 4H-SiC(0001) in nanometer-thick region, *Appl. Phys. Lett.* 104 (2014) 052106.
- [29] T. Hosoi, D. Nagai, M. Sometani, Y. Katsu, H. Takeda, T. Shimura, M. Takei, H. Watanabe, Ultrahigh-temperature rapid thermal oxidation of 4H-SiC(0001) surfaces and oxidation temperature dependence of SiO₂/SiC interface properties, *Appl. Phys. Lett.* 109 (2016) 182114.
- [30] V.V. Afanasev, M. Bassler, G. Pensl, M. Schulz, Intrinsic SiC/SiO₂ interface states, *Phys. Status Solidi A* 162 (1997) 321.
- [31] X. Shen, S.T. Pantelides, Identification of a major cause of endemically poor mobilities in SiC/SiO₂ structures, *Appl. Phys. Lett.* 98 (2011) 053507.